

# Physics Inspired Hybrid Attention for SAR Target Recognition

Zhongling Huang<sup>a</sup>, Chong Wu<sup>a</sup>, Xiwen Yao<sup>a,\*</sup>, Zhicheng Zhao<sup>b</sup>, Xiankai Huang<sup>c</sup> and Junwei Han<sup>a</sup>

<sup>a</sup>the BRain and Artificial Intelligence Lab (BRAIN LAB), School of Automation, Northwestern Polytechnical University, Xi'an, 710072, China

<sup>b</sup>Anhui Provincial Key Laboratory of Multimodal Cognitive Computation, School of Artificial Intelligence, Anhui University, Hefei, 230601, China

<sup>c</sup>Beijing Technology and Business University, Beijing, China

## ARTICLE INFO

### Keywords:

Physical model  
SAR target recognition  
domain knowledge  
hybrid modeling  
explainable artificial intelligence

## ABSTRACT

There has been a recent emphasis on integrating physical models and deep neural networks (DNNs) for SAR target recognition, to improve performance and achieve a higher level of physical interpretability. The attributed scattering center (ASC) parameters garnered the most interest, being considered as additional input data or features for fusion in most methods. However, the performance greatly depends on the ASC optimization result, and the fusion strategy is not adaptable to different types of physical information. Meanwhile, the current evaluation scheme is inadequate to assess the model's robustness and generalizability. Thus, we propose a physics inspired hybrid attention (PIHA) mechanism and the once-for-all (OFA) evaluation protocol to address the above issues. PIHA leverages the high-level semantics of physical information to activate and guide the feature group aware of local semantics of target, so as to re-weight the feature importance based on knowledge prior. It is flexible and generally applicable to various physical models, and can be integrated into arbitrary DNNs without modifying the original architecture. The experiments involve a rigorous assessment using the proposed OFA, which entails training and validating a model on either sufficient or limited data and evaluating on multiple test sets with different data distributions. Our method outperforms other state-of-the-art approaches in 12 test scenarios with same ASC parameters. Moreover, we analyze the working mechanism of PIHA and evaluate various PIHA enabled DNNs. The experiments also show PIHA is effective for different physical information. The source code together with the adopted physical information is available at <https://github.com/XAI4SAR/PIHA>.

## 1. Introduction

Synthetic Aperture Radar (SAR) target recognition has been facilitated by deep learning techniques in recent years. The deep neural networks, for example, can achieve the recognition accuracy of over 99% on the Moving and Stationary Target Acquisition and Recognition (MSTAR) dataset [5] under standard operation condition (SOC) and extended operation conditions (EOC) [4], as shown in Fig. 1 (a). These success stories are grounded in the data-driven nature of the approaches and the straightforward experimental settings.

In addition to attaining greater accuracy for SAR target recognition with more complex deep learning models, there is an increasing demand for the robustness and generalization capability in open environment [3], as well as the interpretability of model design, the consistency of scientific theories, and the awareness of domain knowledge [39; 41]. These requirements have prompted an increase in research efforts aiming at enhancing deep learning models through the integration of prior knowledge into the learning process. It is referred to informed machine learning [50], or theory-guided data science (TGDS) [1].

We preliminarily probe into the integration paradigms of deep neural networks and the physical information of SAR for SAR image interpretation [41; 39]. One of them is the cascade and fusion mode, and another is physics inspired design of model architecture. In the field of SAR target recognition, the physical characteristics of SAR targets, especially the physical parameters of scattering centers, have

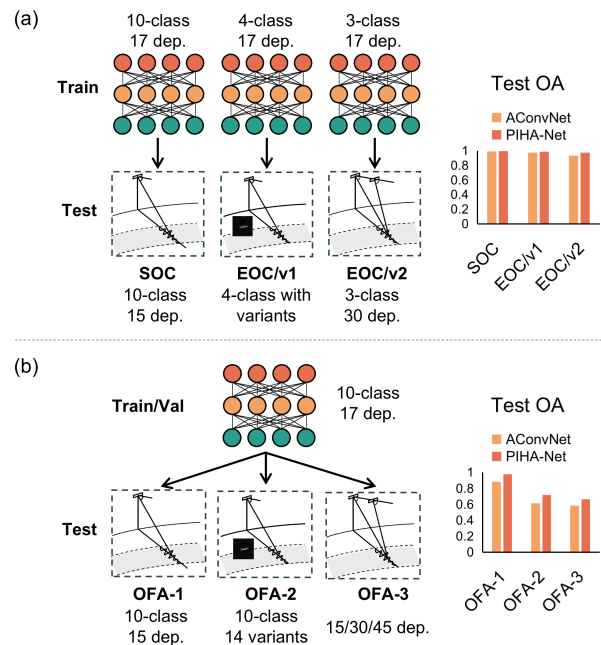


**Figure 1:** The overall accuracy (OA) of both A-ConvNet and the proposed PIHA-Net exhibit very high performance when evaluated using the conventional SOC/EOC setting. However, there is a notable disparity in their results when assessed using the proposed Once-For-All (OFA) evaluation protocol, which was conducted on the MSTAR dataset. The proposed OFA evaluation is more challenging to assess the generalization ability and robustness of a method.

garnered significant attention as an important branch of

\*Corresponding author  
ORCID(s):

domain knowledge [7; 13]. Many recent studies successfully integrate the physical scattering model of SAR into the deep neural networks by considering the ASC parameters of target as an additional data or feature for fusion [10; 43]. However, the model performance is highly influenced by the fixed input physical features. Although the physical features are robust and interpretable, they may be inadaptible for the current task. Besides, the fusion strategy cannot be popularized to adapt various physical information.

To address this issue, we propose to design a knowledge inspired module for SAR target recognition that leverages the physical information in a more flexible way. It can be adaptable to diverse physical information, transferable to arbitrary DNNs, and less influenced by the specific physical feature values.

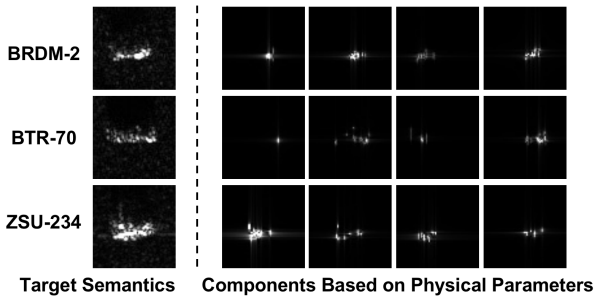


**Figure 2:** On the basis of the physical model, such as the attributed scattering center (ASC), SAR target can be construed as multiple components with local semantics. It provides strong knowledge prior for target recognition.

As shown in Fig. 2, the prominent scattering centers are clustered based on ASC parameters. Each cluster represents a physically explainable component of the target that describes the local semantic, providing rich knowledge prior in recognizing SAR target. Instead of considering the physical parameters as input data or feature, the high-level semantics of physical information are leveraged in this work. We propose the physics inspired hybrid attention (PIHA) mechanism that utilizes the target components shown in Fig. 2 to activate different groups of features and then guide the feature importance re-weighting, making it aware of local semantics. It is flexible to leverage the physical information of SAR target, with the valuable prior resulting in the more contrasting re-weighting of features to influence the outcome. In comparison, the inferior prior will have little impact on feature re-weighting, which prevents performance degradation. PIHA benefits from the flexibility of neural network fitting and the scientificity of the semantic-aware physical information.

In order to evaluate the generalization and robustness of PIHA more effectively, we propose a rigorous evaluation protocol once-for-all (OFA) for the popular MSTAR dataset, i.e., once a deep learning model has been trained and validated on known data, it is evaluated on multiple blind test sets with diverse data distributions. It is more challenging than conventional SOC and EOC evaluation protocols, as

shown in Fig. 1 (b). Notably, many related works have used differing optimization results of the physical model (ASC) to integrate with deep learning for SAR target recognition, which makes it difficult to compare the results with each other fairly. Therefore, we carry out a comparative study based on unified physical information and make it publicly available. In addition, we examine in depth the working mechanism of hybrid attention and summarize the benefits and drawbacks of physical constraints in hybrid modeling. We think that the conclusion can illuminate the design of a deep model that incorporates SAR domain knowledge.

The contributions of our work are summarized as follows:

1. On the basis of knowledge-guided model architecture design, a novel physics-inspired hybrid attention (PIHA) mechanism is proposed for SAR target recognition, in which the semantic prior of physical information is adaptively incorporated with the attention mechanism. It is flexible for different types of physical information and can be incorporated into various deep architectures to enhance performance.
2. In PIHA mechanism, a novel physics-driven attention module named PASE is proposed to utilize the physical information of SAR target for activation and feature re-weighting. The high-level semantics of physical information is leveraged in PASE to ensure the flexibility and generalizability for various physical information.
3. In the experiments, we propose the once-for-all (OFA) evaluation protocol to thoroughly assess the algorithm, demonstrating the robustness and generalization capabilities more effectively. Furthermore, this study delves into the comprehensive examination of the effects of data-driven and physics-driven attentions, offering valuable insights that can serve as a source of inspiration for design concepts.
4. The physical information of SAR targets used in this study together with the source code are open to public, which ensures the reproducibility of our work and facilitates a fair comparison of the results with other methodologies.

In Section 2, we review the related work of SAR target recognition approaches that integrate the physical model and deep neural networks for hybrid modeling, as well as the attention mechanism in computer vision filed. The proposed PIHA module is introduced in Section 3. Section 4 presents the experiments and discussions and the conclusion is given in Section 5.

## 2. Related Work

### 2.1. SAR Target Recognition with Hybrid Modeling

Compared to optical images, SAR images possess a number of distinct characteristics, which can be described by some physical models such as attributed scattering center or the specific data format like phase information in complex data. We define the approaches integrating the physical model

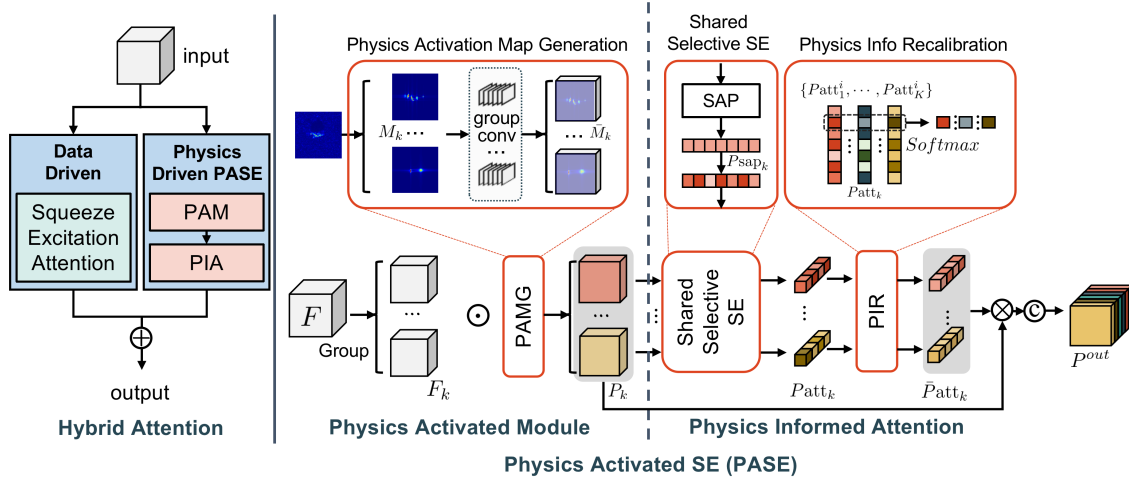


**Figure 3:** The proposed physics-inspired hybrid attention (PIHA) is a combination of data-driven and physics-driven attention PASE. The physics-activated squeeze and excitation module (PASE) is composed of physics activated module (PAM) and physics-informed attention (PIA).

or physical information of SAR with deep neural networks as hybrid modeling [39].

The most prevalent and efficient method is feature fusion with a cascaded physical model in a neural network. The principle concern is the representation of the physical model. For example, based on ASC model, the previous work applied the bag of words (BoW) [7], point cloud [19], as well as the reconstruction part image [16], to represent the ASC parameters as efficient features that can be easily fused with image features. The other concern is the fusion approach, including early fusion (data), mid-level fusion (feature), and late fusion (decision). For instance, the feature fusion based on discriminant correlation analysis (DCA) [7], cross attention [13], concatenate or addition of global image feature and part image features [9], adaptive weighting fusion [15], multi-manifold fusion of amplitude and phase features [10], and fusion in decision level [14].

The other hybrid modeling paradigm is physics inspired or physics guided model design for SAR target recognition [41]. Karpatne et al. [1] proposed the theory-guided data science (TGDS) paradigm, including the theory-guided design of model architecture in which scientific knowledge is used to influence the architecture of data science model. In SAR target recognition field, Liu et al. [6] proposed to initialize the model weights based on ASC parameters. Feng et al. [17] designed a physics guided neural network to embed the scattering center knowledge into feature representation motivated by [42].

The success of feature fusion-based hybrid modeling approaches is primarily dependent on the high representation capacity of physical features and the efficacy of the fusion strategy. It is less adaptable to various physical characteristics. For algorithm development, the physics-guided model design is more interpretable and transparent. Both of them can achieve more robust and generalized model.

## 2.2. Attention Mechanism in Deep Learning

The attention mechanism attempts to imitate the human visual ability and cognitive system in order to focus on the significant information of the image. SE [23] proposed channel attention to reweight the feature in each channel. ECA-Net [24] adopted an 1D convolution to decrease the complexity of generating channel attention. Further, SK-Net [25] and EPSANet [26] split feature along channel dimension and process feature with kernel of different size to acquire multiscale channel attention. A2-Nets [27] introduced a novel function to capture the global relation of spatial information. CBAM [28] and BAM [29] enriched the attention map by combining the channel attention and spatial attention. DANet [30] applied the self-attention mechanism on channel attention and spatial attention to model long-range dependency. SANet [31] split the feature along the channel dimension and adopt channel attention and spatial attention on each group.

The above mentioned methods aim to optimize the structure of channel and spatial attention to achieve better performance. The calculation of attention is solely dependent on the given feature map, and we summarize them as data-driven attention. Another feasible way is combining attention with prior knowledge. Hao et al. [32] applied a pre-trained embedding matrix, which contains the information of a large knowledge base, to build the cross attention model in question answering task. He et al. [33] adopted TransE [47] to embed the marine knowledge graph into a self-attention module in named entity recognition task. In medical image classification, PKA2-Net [34] generated a series of templates on principle of energy decay to obtain the attention feature. In heart disease prediction, MINA [35] combined the prior medical knowledge [48; 49] to compute attention weights.

The data-driven attention is flexible and adaptive, while the knowledge integrated attention is aware of prior information. In order to take the advantage of both, we propose the hybrid attention PIHA in this paper.

### 3. Method

In this section, we first introduce the overall structure and design idea of the proposed PIHA. Then, the details of the data-driven and physics-driven block, named physics activated squeeze and excitation (PASE) module, is illustrated. Finally, we present how to design a PIHA enabled deep neural network.

#### 3.1. PIHA Overview

The physical information of SAR target is robust but less flexible and may be not exactly to the benefit of recognition. Different from the most hybrid modeling methods that consider the physical information as an input data or feature for fusion, the proposed method leverages the high-level semantics provided by physical information to re-weight features. PIHA is a combination of data-driven and physics-driven blocks, as shown in Fig. 3, that regulates the impact of semantic prior adaptively. The physics-driven block, denoted as physics activated squeeze and excitation (PASE), aims to activate and re-weight the feature groups by means of knowledge prior to make them aware of local semantics. The valuable prior results in contrasting feature re-weighting that highlight important features to influence the result. The data-driven SE attention dominates when knowledge prior is inferior. The design ensures the positive impact of physical information and improves the flexibility of applying physical information. Besides, PIHA is a general module that can be inserted to any level of DNNs and adapts different physical models.

Let  $F \in \mathbb{R}^{C \times H \times W}$  denotes the input feature, where  $C, H, W$  represent channel, height, weight respectively. The data-driven attention implemented by a SE block [23] aims to re-weight the feature map  $F$  based on the global visual information, obtaining  $D^{out}$ . On the other hand, the physics-driven attention, denoted as PASE module, respectively enhances the feature  $F$  based on the local semantics of physical information and outputs  $P^{out}$ . The eventual output of PIHA is denoted as:

$$F_{PIHA} = D^{out} + P^{out}, \quad (1)$$

as the fusion of data-driven and physics-driven outputs.

#### 3.2. Data-Driven SE

The data driven SE block consists of squeeze and excitation for decoding the global spatial information and re-calibrating weights of each channel, which can be referred to literature [23]. First, global average pooling is adopted to squeeze the spatial information:

$$D_c^{sq} = \frac{1}{H \times W} \sum_{i=1}^H \sum_{j=1}^W F_c(i, j) \quad (2)$$

**Table 1**

The combination of  $\alpha$  and  $L$  defines canonical types of scattering centers.

Scattering geometry	$\alpha$	$L$
Trihedral	1	$L = 0$
Top Hat	0.5	$L = 0$
Corner diffraction	-1	$L = 0$
Sphere	0	$L = 0$
Edge broadside	0	$L > 0$
Edge diffraction	-0.5	$L > 0$
Dihedral	1	$L > 0$
Cylinder	0.5	$L > 0$

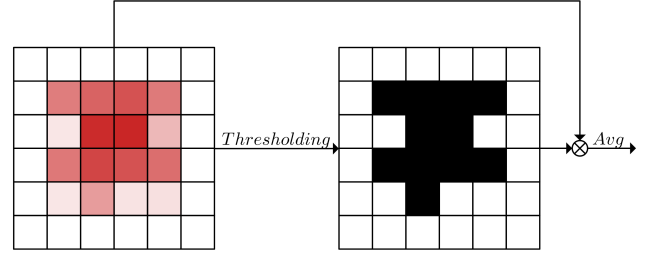


**Figure 4:** Illustration of selective average pooling.

where  $F_c$  denotes the  $c$ -th channel of input feature. Then, a bottleneck with two fully-connected layers, i.e. a dimensionality-reduction layer and a dimensionality-increasing layer, are adopted to generate channel attention  $D^{attn} \in \mathbb{R}^{C \times 1 \times 1}$ :

$$D^{attn} = \sigma(W_1 \delta(W_0(D^{sq}))) \quad (3)$$

where  $W_1 \in \mathbb{R}^{\frac{C}{r} \times C}$  and  $W_0 \in \mathbb{R}^{C \times \frac{C}{r}}$ .  $\delta$  represents Rectified Linear Unit (ReLU) [44] operation and  $\sigma$  is excitation function where Sigmoid is usually used. Finally, the input feature is recalibrated by the channel attention:

$$D^{out} = D^{attn} \otimes F \quad (4)$$

where  $\otimes$  refers to the channel-wise multiplication.

#### 3.3. Physics-Driven PASE

The physics-driven PASE consists of the physics activated module (PAM) and the physics informed attention (PIA).

As shown in Fig. 2, the target components based on ASC physical model provide rich local semantics that should be valuable for recognizing different targets. Regarding it as a robust prior, PASE is proposed by introducing the physical information to architecture design, achieving physics-aware attentions based on local semantics of target components. Hence, the feature map is re-weighted with channel-wise physics specificity to enhance the generalization capability and robustness.

The proposed PASE is cascaded by PAM and PIA, where PAM activates the spatial information of each subgroup features based on the target component obtained with physical information, and PIA models the channel

importance of each sub-group features with local semantics and enhances the interaction of different local semantics using the physical information re-calibration (PIR) cell.

### 3.3.1. Knowledge based Target Components

In this work, we mainly apply the ASC physical model to generate the target components with physical meanings. Based on the high-frequency approximations, the radar backscattering of a target can be approximated by a set of points. From Gerry's theory [54], each scattering center can be represented by seven parameters which is named attributed scattering center. Thus, the target backscattering is parameterized on the basis of geometrical theory of diffraction (GTD) as:

$$E(f, \varphi; \Theta) = \sum_{i=1}^q A_i \cdot \left(j \frac{f}{f_c}\right)^{\alpha_i} \cdot \exp(2\pi\gamma_i f \sin \varphi) \cdot \exp[-j4\pi \frac{f}{c}(x_i \cos \varphi + y_i \sin \varphi)] \cdot \text{sinc}(2\pi \frac{L_i}{c} f \sin(\varphi - \bar{\varphi}_i)) \quad (5)$$

where  $f$  and  $\varphi$  denote the frequency and aspect angle, while  $f_c$ ,  $c$  and  $q$  denote the center frequency, propagation velocity of electromagnetic wave, and the number of scattering centers, respectively.  $\Theta$  is the physical parameter set of scattering centers containing  $(A, x, y, \alpha, L, \bar{\varphi}, \gamma)$ , that are, amplitude  $A$  of echos, relative position  $(x, y)$ , frequency dependence  $\alpha$ , length  $L$ , orientation  $\bar{\varphi}$ , and aspect dependency  $\gamma$ . The combination of  $\alpha$  and  $L$  decides the type of scattering centers, as shown in Table 1.

The estimated physical parameter set  $\hat{\Theta}$  is obtained by solving the following optimization problem:

$$\hat{\Theta} = \arg \min_{\Theta} \|S(f, \varphi) - E(f, \varphi; \Theta)\|_2 \quad (6)$$

where  $S(f, \varphi)$  is the signal in frequency domain. In our work, the optimization problem is solved by orthogonal matching pursuit (OMP) algorithm [51].

Then, the target components are generated based on the estimated physical parameter  $\hat{\Theta}$ . Following the statistical method in literature [7], the bag of visual words (BOVW) representation is adopted to process the ASC feature, followed by K-means clustering to obtain K groups of parameter set, denoted as  $\{\Theta_i^{(1)}\}_{i=1}^{N_1}, \dots, \{\Theta_i^{(K)}\}_{i=1}^{N_K}$ , where  $N_k$  denotes the number of the  $k$ th cluster. Finally, the physical parameters in each group is reconstructed to SAR image domain to obtain K images with target components, denoted as  $M_1, \dots, M_K$ .

In the experiments, we compare the results of applying different parameters in  $\Theta$  for clustering, including  $\{x, y, L, \bar{\varphi}, \alpha, A\}$ ,  $\{x, y, A\}$ , and  $\{x, y\}$ . Apart from ASC model which requires the complex-valued SAR image, we can also adopt other approaches to generate the target components, as shown in Fig. 6, which will be further discussed in the experiments.

### 3.3.2. Physics Activation Module

In order to attain the features aware of different local semantics, the input feature  $F$  is firstly split into K groups  $(F_1, \dots, F_K)$  and then activated respectively on the basis of the obtained target components  $M_k$ . As shown in Fig. 3, the physics activation map  $\bar{M}_k$  is generated by a group of convolutions on each  $M_k$ , denoted as:

$$\bar{M}_k = \text{Conv}_k(M_k) \quad (7)$$

where  $\text{Conv}_k$  is the  $k$ -th group convolution layer with a kernel number of  $\frac{C}{K}$ . In this way, the processed physics activation map  $\bar{M}_k$  is with the size of  $\frac{C}{K} \times H \times W$ , as same as  $F_k$ . The group convolution operation preserves the local semantics of each  $M_k$  while simultaneously refining the feature in each channel within a group. Then, the physics activated group feature emphasizing each target component is obtained by the element-wise product of  $\bar{M}_k$  and  $F_k$ :

$$P_k = \bar{M}_k \odot F_k \quad (8)$$

### 3.3.3. Physics Informed Attention

The objective of the PIA module is to re-weight the importance of features based on the local semantics of targets (SSE). Additionally, it aims to facilitate the interaction of local semantics among channels, thereby enhancing their informativeness (PIR).

The conventional global average pooling (GAP) layer in the SE module takes into consideration the entire spatial information of features, which will cause the background to dominate the GAP result in the SAR target image. As a consequence, we propose a shared selective SE (SSE) module to concentrate on the primary semantic regions. The squeezed feature is obtained by a selective average pooling (SAP) layer instead of GAP, as shown in Fig. 4, where a threshold is defined to determine whether to preserve in  $P_k$  to calculate the average pooling value.

For each sub-group feature  $P_k$  with  $\frac{C}{K}$  channels, the selective mask of the  $i$ -th feature within  $P_k$  is denoted as  $\text{Mask}_k^{(i)}$ . It is obtained based on a defined threshold  $\rho$ :

$$\text{Mask}_k^{(i)} = \begin{cases} 1, & P_k^{(i)} \geq \rho \\ 0, & P_k^{(i)} < \rho \end{cases} \quad (9)$$

Then, the selective average pooling of each feature is realized by:

$$P_{\text{sap}_k}^{(i)} = \frac{\sum_{H \times W} \text{Mask}_k^{(i)} \odot P_k^{(i)}}{\sum_{H \times W} \text{Mask}_k^{(i)}} \quad (10)$$

The  $k$ -th sub-group output of SSE is achieved by a MLP layer as same as Equation (3):

$$\text{Pattn}_k = \sigma(W_1 \delta(W_0(P_{\text{sap}_k})) \quad (11)$$

Further, in order to establish the interaction between different local semantics, we design the physical information recalibration (PIR) implemented by a Softmax layer along the axis

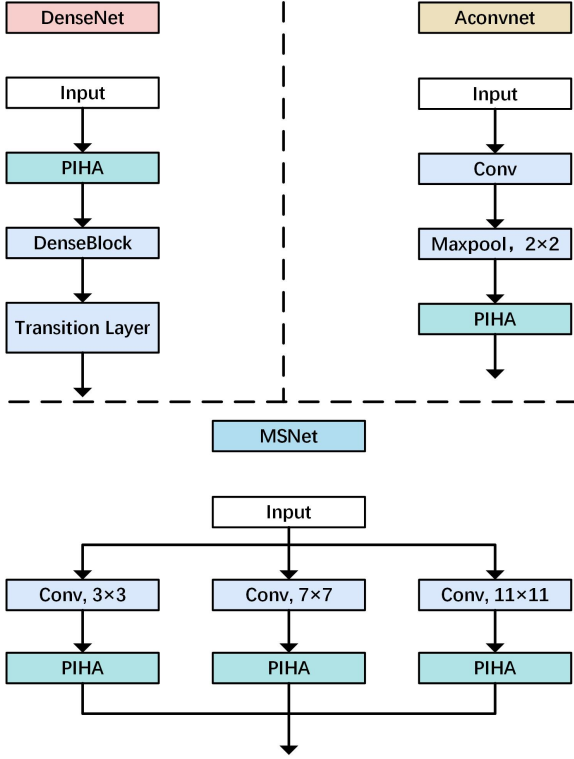


**Figure 5:** Structure of PIHA enabled deep model.

of target components:

$$\bar{P}att_1^i, \dots, \bar{P}att_K^i = \text{Softmax}(Patt_1^i, \dots, Patt_K^i) \quad (12)$$

$$i = 1, 2, \dots, \frac{C}{K}$$

where  $\bar{P}att_k^i$  is the  $i$ -th attention in the  $k$ -th sub-group. PIR re-calibrates channel weight in order to interact the local semantics of various target components across channels. Finally, the output features of the PASE module  $P^{out}$  can be obtained by:

$$P_k^{out} = P_k \otimes \bar{P}att_k \quad (13)$$

$$P^{out} = \text{Concat}(P_1^{out}, P_2^{out}, \dots, P_K^{out}) \quad (14)$$

The aforementioned PASE attention method incorporates the physical information of the target as a robust prior, which not only activates the feature map to extract local sub-group features with semantic awareness but also aids in generating channel weights associated with the target component.

### 3.4. PIHA Enabled DNN

The proposed PIHA can be embedded in different deep neural networks. In our work, three different backbones are explored, as illustrated in Fig. 5. Generally, PIHA is inserted after feature processing blocks such as convolution and max-pooling layers. For A-ConvNet [4], it is placed after every max-pooling layer. In DenseNet-121 [52], the proposed

PIHA is followed by each DenseBlock and Transition Layer. In a multi-stream neural network such as MS-Net [21], PIHA is inserted after the convolution layer in each stream for the purpose of introducing physical information at different scales. By adaptively incorporating physics-aware semantics information, the PIHA-enabled deep neural network inherits the benefits of the original backbone and enhances its robustness and generalization capacity.

## 4. Experiments

### 4.1. Experimental Settings

#### 4.1.1. Once for All Evaluation Protocol

Our experiments are mainly conducted on the MSTAR dataset [5] with the proposed once for all (OFA) evaluation protocol.

The current deep learning based approaches can achieve very high performance on the traditional evaluation protocol, i.e., standard operation condition (SOC) and extended operation condition (EOC). Fig. 1 shows the proposed PIHA-Net and the A-ConvNet performs 99.38% and 99.25% on SOC, 98.73% and 97.36% on EOC (version variants) respectively. There is limited scope for improving the performance of an algorithm based on the traditional evaluation protocol, hence diminishing the significance of the assessment. To this end, we propose a more rigorous OFA evaluation process.

Once for all denotes that, once the model has been trained and validated with known data, it is evaluated on multiple test sets with varying data distributions. It differs from the conventional SOC and EOC evaluations, which train multiple models to fit various test sets. OFA can more effectively evaluate the robustness and generalization capability of an algorithm.

The MSTAR dataset is collected by Sandia National Laboratory's SAR sensor operating at X-band and HH polarization. It contains several types of static military vehicles with variants, consisting of a full range of orientation angles and different depression angles. As shown in Table 2, the samples observed in the depression angle of  $17^\circ$  are regarded as known data for training and validation. To evaluate the algorithm in the abundant and limited training data cases respectively, we randomly select 90%, 50%, 30%, and 10% samples as training set and correspondingly using 10%, 50%, 50%, and 50% samples in the rest  $17^\circ$  depression angle data as validation set, respectively.

The proposed OFA evaluation protocol contains three test scenarios. OFA-1 indicates that the test set has a similar data distribution to the training and validation sets, with the same types and serial numbers and a similar depression angle of  $15^\circ$ . OFA-2 introduces four additional variants in BMP-2 and T-72 compared to OFA-1, 3203 samples in total. OFA-2 evaluates the robustness of recognition algorithms to various variants. OFA-3 is a mixture of different depression angles containing  $15^\circ$ ,  $30^\circ$ , and  $45^\circ$ , where only three categories are included with 3093 samples in total. There is a significant distribution drift in OFA-3 compared with training and validation set that makes the task more challenging.

**Table 2**

The once-for-all (OFA) evaluation protocols for MSTAR dataset.

Class	Train/Val			OFA-1			OFA-2			OFA-3		
	Serial	Dep.	No.	Serial	Dep.	No.	Serial	Dep.	No.	Serial	Dep.	No.
BMP-2	9563	17°	233	9563	15°	195	9563	15°	195	/	/	/
	/	/	/	/	/	/	9566	15°	196	/	/	/
	/	/	/	/	/	/	C21	15°	196	/	/	/
BTR-70	C71	17°	233	C71	15°	196	C71	15°	196	/	/	/
T-72	132	17°	232	132	15°	196	132	15°	196	/	/	/
	/	/	/	/	/	/	812	15°	195	/	/	/
	/	/	/	/	/	/	S7	15°	191	/	/	/
BTR-60	k10yt7532	17°	256	k10yt7532	15°	195	k10yt7532	15°	195	/	/	/
2S1	b01	17°	299	b01	15°	274	b01	15°	274	b01	15°/30°/45°	274/288/303
BRDM-2	E-71	17°	298	E-71	15°	274	E-71	15°	274	E-71	15°/30°/45°	274/420/423
D7	92v13015	17°	299	92v13015	15°	274	92v13015	15°	274	/	/	/
T-62	A51	17°	299	A51	15°	273	A51	15°	273	/	/	/
ZIL-131	E12	17°	299	E12	15°	274	E12	15°	274	/	/	/
ZSU-234	d08	17°	299	d08	15°	274	d08	15°	274	d08	15°/30°/45°	274/406/422
<b>Total</b>	2747			2425			3203			3093		

**Table 3**

Ablation studies conducted on DenseNet121 and A-ConvNet backbones.

Backbone	Data-Driven	Physics-Driven		90			50		
	SE	PAM	PIR	OFA-1	OFA-2	OFA-3	OFA-1	OFA-2	OFA-3
DenseNet121	✗	✗	✗	95.37±1.04	91.73±0.76	60.37±2.66	91.60±1.82	88.45±1.58	60.18±1.57
	✓	✗	✗	95.87±1.50	93.20±1.46	61.55±2.33	92.54±1.21	88.97±1.20	60.84±1.83
	✗	✓	✓	78.86±4.31	74.09±4.4	50.67±2.1	66.8±1.63	62.62±2.05	48.05±0.91
	✓	0.25	0	96.87±0.83	93.27±1.15	60.99±3.17	<b>95.53±0.38</b>	91.93±0.38	58.35±3.77
	✓	✓	✓	<b>97.41±0.99</b>	<b>94.4±1.66</b>	<b>62.07±2.4</b>	95.32±1.3	<b>91.97±1.72</b>	<b>61.81±1.16</b>
A-ConvNet	✗	✗	✗	86.95±5.69	84.51±6.06	57.16±3.07	92.48±5	88.88±4.82	62.8±2.31
	✓	✗	✗	86.18±5.01	83.9±3.12	57.24±2.57	92.89±1.32	88.74±2.63	57.86±2.78
	✗	✓	✓	90.96±3.84	87.48±2.76	57.28±0.84	<b>93.71±4.91</b>	<b>89.94±5.04</b>	<b>63.87±4.45</b>
	✓	0.25	0	89.53±7.44	86.98±7.32	57.83±5.3	90.66±3.76	87.66±3.84	59.41±3.24
	✓	✓	✓	<b>94.96±2.84</b>	<b>93.02±3.24</b>	<b>57.91±1.8</b>	93.13±3.24	89.06±3.54	59.11±2.89
Backbone	Data-Driven	Physics-Driven		30			10		
	SE	PFM	PAM	OFA-1	OFA-2	OFA-3	OFA-1	OFA-2	OFA-3
DenseNet121	✗	✗	✗	84.72±1.13	80.29±1.21	57.44±2.56	65.58±3.49	59.32±3.21	<b>56.63±3.18</b>
	✓	✗	✗	84.54±1.08	80.52±0.93	57.00±1.58	64.98±3.01	58.87±3.36	54.38±2.06
	✗	✓	✓	55.12±2.68	51.98±2.54	41.94±1.68	41.58±0.82	38.96±0.35	35.69±1.36
	✓	0.25	0	89.48±1.01	85.6±1.08	60.13±1.24	70.71±2.37	65.16±1.78	54.01±2.19
	✓	✓	✓	<b>90.2±1.43</b>	<b>85.98±1.73</b>	<b>61.91±1.45</b>	<b>71.97±1.97</b>	<b>65.89±2.08</b>	53.87±1.85
A-ConvNet	✗	✗	✗	87.65±2.39	83.04±3.32	58.63±1.73	72.02±1.7	64.76±2.27	52.71±2.28
	✓	✗	✗	90.38±2.85	85.1±3.38	<b>59.44±2.92</b>	73.53±4.32	66.82±3.46	<b>54.07±4.18</b>
	✗	✓	✓	82.62±2.14	76.23±2.27	56.8±1.52	62.22±3.11	56.73±3.23	49.11±1.36
	✓	0.25	0	90.94±2.56	85.76±2.24	59.27±2.65	<b>76.17±2.36</b>	68.9±3.41	50.38±2.34
	✓	✓	✓	<b>91.18±2.19</b>	<b>86.49±2.49</b>	58.78±1.03	76.11±1.93	<b>69.6±2.95</b>	53.22±1.56

Consequently, OFA-3 evaluates the generalization capability of recognition algorithm to different observation conditions.

#### 4.1.2. Implementation Details

The target image chips are center cropped to 128×128. The threshold  $\rho$  in SAP is set to 0.05. The network parameters are randomly initialized without pre-training and the data augmentation is deactivated. The learning rate is set to 5e-4, 5e-3, and 5e-4 for DenseNet121 [52], A-ConvNet [4], and MS-Net backbones, respectively. The batchsize is 32. Stochastic gradient descent (SGD) is applied with

momentum rate of 0.9 and weight decay of 0.001. A strategy of early stopping is implemented, which entails ceasing training if the accuracy of the validation set does not improve within 200 epoch. The utmost number of training epochs is 1000. Each experiment is repeated five times in order to record the mean and standard deviation.

## 4.2. Ablation Studies

In this section, we report ablation study results based on DenseNet-121 and A-ConvNet backbones, two representative architectures of deep and shallow neural networks, to investigate the effectiveness of PIHA module.

### 4.2.1. Data-driven SE

The original SE block aims to recalibrate the feature importance among channels. The SE weights are determined by the global information of feature maps. Table 3 reported the performance of the baseline backbone and the SE-Net counterpart in the first and second row. Noted that when sufficient training data is available, the deeper model outperforms the shallow model, whereas the shallow architecture performs better when training data is scarce. Interestingly, we can observe that the data-driven SE block improves the performance of deeper architecture with sufficient training data, and the shallow architecture with insufficient training data, more significantly than the other cases.

### 4.2.2. Physics-aware SE

When only physics-driven attention is enabled, as shown in the third row in Table 3, the performance of shallow and deeper architectures differs significantly. DenseNet-121 fails with only PASE module, whereas A-ConvNet improves when trained with 90% and 50% of the data, but fails with very few training examples. As a comparison, the combination of PASE and data-driven SE improves the performance. The phenomenon manifest the different working mechanism of data-driven and physics-aware attentions. PASE module provides strong knowledge prior of local semantics related to target components, and the trainable parameters in PASE enable the physical priors to be more adaptable and flexible during the optimization process. The very limited training samples, as well as the very deep layer-wise information process, will result in more strict constraint of physical priors with losing accuracy. Therefore, the combination of knowledge aware PASE and flexible data-driven SE collaborate to improve the performance of DenseNet-121 significantly.

### 4.2.3. Physical information Recalibration

The proposed physics informed attention in the designed PASE module includes: SSE to reweight the feature map within each target component, and PIR to establish the interaction among different components. Table 3 reported the effectiveness of the proposed PIR by comparing the results in the fourth and fifth row. The parameters 0.25 and 0 indicate that the output of SSE is multiplied by 0.25 to acquire the final PASE attention without PIR for the purpose of comparing the performance of enabling PIR with Softmax under the condition of four target components. It can be inferred from the results that the interaction between components can further enhance the performance in most cases.

## 4.3. Effectiveness of PIHA on Different Architectures

To evaluate the effectiveness of the proposed PIHA module, we apply different backbones with PIHA modules as illustrated in Section 3.4. The results are given in Table 4, where DenseNet-121 [52], A-ConvNet [4], and MS-Net are explored. MS-Net is modified on the basis of MS-CVNETs [21] where we replace the complex-valued layers with real number structure and deepen the channel of feature. The specific definition of models can be found at <https://github.com/XAI4SAR/PIHA/model/>.

The results are recorded in Table 4, where the robustness and generalization ability of the algorithm are comprehensively evaluated on the condition of abundant and limited data. The PIHA enabled neural network can achieve better performance than the original one in most cases. The effectiveness of PIHA on different architectures can be proved.

## 4.4. Comparative Study with SOTA Methods

We compare the proposed PIHA enabled deep model based on MS-Net architecture (MS-PIHA) with other SAR target recognition approaches, including the data-driven real-valued neural network (ResNet-18 [53], A-ConvNet [4]), complex-valued neural network (MS-CVNETs [21]), and the hybrid modeling approaches integrating ASC model (FEC [7], ESF [17], CA-MCNN [22]). To make the comparison fair enough, we apply the same ASC optimization results with our work and all experiments follow the proposed OFA evaluation protocols. The results are recorded in Table 5, where \* represents our implementations since there is no publicly available source code. The hyper-parameter setting follows the original papers. All models were trained without any data augmentation.

As shown in Table 5, the OFA evaluation results of the comparative methods are not as good as those presented in the original papers evaluated on SOC and EOC. This indicates the proposed OFA evaluation is more rigorous and makes the task more challenging, allowing a more reliable assessment of generalization capability and robustness. The proposed MS-PIHA scores 8 first-place and 4 second-place results in terms of the mean value of the results among the twelve test scenarios, and achieves smaller fluctuation compared with the four first-place results. In the most challenging case of OFA-3 with 10% training data, our method outperforms the second-best result by 7.52%. It also outperforms other hybrid modeling methods with the same ASC parameters. The variability in performance among three hybrid modeling approaches (FEC, ESF, CA-MCNN) with the same ASC settings indicates that the outcomes of the algorithm are significantly influenced by the results of the physical model. As a comparison, the proposed PIHA enabled model leverages the semantic prior of physical parameters rather than their specific values, resulting in enhanced performance with increased adaptability and flexibility.

**Table 4**

The performance comparison of different backbones and their PIHA enabled versions.

Model	90			50		
	OFA-1	OFA-2	OFA-3	OFA-1	OFA-2	OFA-3
DenseNet121	95.37±1.04	91.73±0.76	60.37±2.66	91.60±1.82	88.45±1.58	60.18±1.57
+ PIHA	<b>97.41±0.99</b>	<b>94.4±1.66</b>	<b>62.07±2.4</b>	<b>95.32±1.3</b>	<b>91.97±1.72</b>	<b>61.81±1.16</b>
A-ConvNet	86.95±5.69	84.51±6.06	57.16±3.07	92.48±5	88.88±4.82	<b>62.8±2.31</b>
+ PIHA	<b>94.96±2.84</b>	<b>93.02±3.24</b>	<b>57.91±1.8</b>	<b>93.13±3.24</b>	<b>89.06±3.54</b>	59.11±2.89
MS-Net	97.91±0.94	95.33±0.87	64.2±2.03	97.44±0.24	<b>94.41±0.55</b>	65.84±0.58
+ PIHA	<b>98.22±0.38</b>	<b>96.22±0.65</b>	<b>66.1±3.09</b>	<b>97.59±0.23</b>	94.36±0.54	<b>66.47±1.35</b>

Backbone	30			10		
	OFA-1	OFA-2	OFA-3	OFA-1	OFA-2	OFA-3
DenseNet121	84.72±1.13	80.29±1.21	57.44±2.56	65.58±3.49	59.32±3.21	<b>56.63±3.18</b>
+ PIHA	<b>90.2±1.43</b>	<b>85.98±1.73</b>	<b>61.91±1.45</b>	<b>71.97±1.97</b>	<b>65.89±2.08</b>	53.87±1.85
A-ConvNet	87.65±2.39	83.04±3.32	58.63±1.73	72.02±1.7	64.76±2.27	52.71±2.28
+ PIHA	<b>91.18±2.19</b>	<b>86.49±2.49</b>	<b>58.78±1.03</b>	<b>76.11±1.93</b>	<b>69.6±2.95</b>	<b>53.22±1.56</b>
MS-Net	92.94±0.73	88.33±0.82	63.9±2.35	78.43±0.73	<b>72.81±1.01</b>	59.82±0.77
+ PIHA	<b>93.41±0.83</b>	<b>89.31±0.9</b>	<b>64.88±1.22</b>	<b>78.56±0.74</b>	72.49±0.37	<b>60.23±0.98</b>

**Table 5**

The comparative study with some state-of-the-art methods. Note that \* is our implementation, as there is no publicly available source code. All hybrid modeling methods apply the unified physical parameters of ASC model optimized by OMP algorithm. **Bold** and Underline highlight the best and the second best result, respectively.

Method	Modeling	Input	90			50		
			OFA-1	OFA-2	OFA-3	OFA-1	OFA-2	OFA-3
ResNet18	data-driven	amplitude	90.22±6.98	89.5±6.92	52.28±5.71	<u>93.94±1.96</u>	<u>93.05±2.22</u>	56.82±1.73
A-ConvNet*	data-driven	amplitude	86.95±5.69	84.51±6.06	57.16±3.07	<u>92.48±5</u>	88.88±4.82	<u>62.8±2.31</u>
FEC*	hybrid	complex	92.32±4.41	86.22±5.03	58.76±5.18	86.23±5.62	81.34±5.83	55.03±2.35
ESF*	hybrid	amplitude	89.81±5.08	85.37±6.03	57.98±1.88	91.68±3.53	88.61±3.03	54.04±4.53
CA-MCNN*	hybrid	complex	94.56±2	92.76±1.72	49.35±5.07	93.34±3.08	91.56±2.37	51.81±4.23
MS-CVNETs	data-driven	complex	96.77±1.74	94.34±1.22	<b>66.83±3.96</b>	93.43±1.89	90.78±1.83	62.56±3.71
MS-PIHA (Ours)	hybrid	flexible	<b>98.22±0.38</b>	<b>96.22±0.65</b>	<u>66.1±3.09</u>	<b>97.59±0.23</b>	<b>94.36±0.54</b>	<b>66.47±1.35</b>

Method	Modeling	Input	30			10		
			OFA-1	OFA-2	OFA-3	OFA-1	OFA-2	OFA-3
ResNet18	data-driven	amplitude	92.08±3.25	<b>90.23±3.34</b>	50.4±1.05	71.67±6.19	67.37±4.44	40.78±5.8
A-ConvNet*	data-driven	amplitude	87.65±2.39	83.04±3.32	<u>58.63±1.73</u>	72.02±1.7	64.76±2.27	<u>52.71±2.28</u>
FEC*	hybrid	complex	68.43±7.72	64.48±6.16	51.12±1.81	57.84±3.47	54.04±3.91	43.44±5.97
ESF*	hybrid	amplitude	89.38±1.47	85.26±1.79	56.82±1.43	75.92±4.79	71.31±3.96	50.21±5.69
CA-MCNN*	hybrid	complex	90.99±1.11	86.6±1.5	52.72±2.94	<b>80.02±1.48</b>	<b>73.19±1.08</b>	44.18±1.21
MS-CVNETs	data-driven	complex	81.33±0.95	77.5±0.97	56.02±1.11	49.11±4.27	44.63±3.74	38.96±5.78
MS-PIHA (Ours)	hybrid	flexible	<b>93.41±0.83</b>	<u>89.31±0.9</u>	<b>64.88±1.22</b>	<u>78.56±0.74</u>	<u>72.49±0.37</u>	<b>60.23±0.98</b>

Note that the data-driven method MS-CVNETs, taking the complex-valued data as the input, achieve remarkable results with sufficient training data. With very limited training samples, i.e., only 10% for training, the hybrid modeling methods, such as CA-MCNN and our PIHA enabled MS-Net, show superiority compared with data-driven approaches.

In conclusion, hybrid modeling approaches that use physical information of SAR demonstrate a distinct advantage over data-driven methods when dealing with extremely limited labeled data. The physical information of SAR, such as physical parameters that describe target characteristics, provides strong knowledge prior. However, it exhibits limited

flexibility and adaptability, since the model performance heavily depends on the quality of the physical information. The knowledge prior guided model design can be more flexible to leverage the physical information of high quality while mitigating the impact of irrelevant prior.

#### 4.5. Physical Information Discussion

In this section, we discuss the effectiveness of PIHA on the basis of different physical information. The ASC model, for example, contains several physical parameters to represent scattering centers. We generate the target components based on different combination of the physical

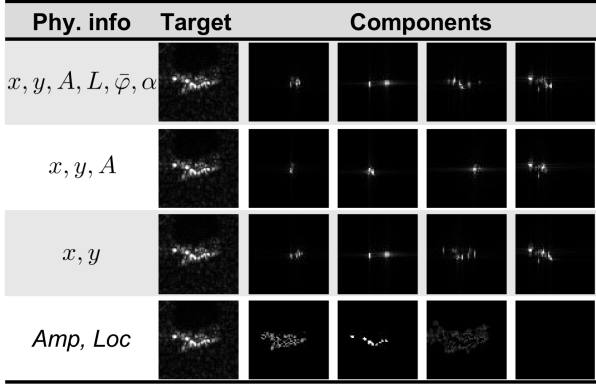
**Table 6**

The performance of PIHA module with various physical information.

Model	Physics Basis	90			50		
		OFA-1	OFA-2	OFA-3	OFA-1	OFA-2	OFA-3
DenseNet-121	None	95.37±1.04	91.73±0.76	60.37±2.66	91.60±1.82	88.45±1.58	60.18±1.57
+PIHA w/o ASC	Amp, Loc	96.5±1.57	92.76±1.6	<b>63.13±1.62</b>	95.38±0.92	91.01±1.15	60.45±1.69
+PIHA w/ ASC	$x, y$	96.65±0.99	93.36±0.87	62.92±3.26	94.59±1.17	90.52±1.8	60.99±2.01
	$x, y, A$	96.87±1.37	93.51±1.5	62.81±2.08	<b>95.48±0.79</b>	91.68±0.41	60.89±2.22
	$x, y, L, \bar{\varphi}, \alpha, A$	<b>97.41±0.99</b>	<b>94.4±1.66</b>	62.07±2.4	95.32±1.3	<b>91.97±1.72</b>	<b>61.81±1.16</b>

Model	Physics Basis	30			10		
		OFA-1	OFA-2	OFA-3	OFA-1	OFA-2	OFA-3
DenseNet-121	None	84.72±1.13	80.29±1.21	57.44±2.56	65.58±3.49	59.32±3.21	<b>56.63±3.18</b>
+PIHA w/o ASC	Amp, Loc	88.74±0.92	84.76±0.96	59.26±1.94	70.11±4.16	64.86±3.55	51.95±1.75
+PIHA w/ ASC	$x, y$	90.15±0.95	85.94±1.79	60.78±4.04	70.75±2.36	65.18±2.03	54.51±2.07
	$x, y, A$	88.88±1.54	84.75±2.01	61.11±1.9	71.33±3.9	65.98±4.18	53.66±3.26
	$x, y, L, \bar{\varphi}, \alpha, A$	<b>90.2±1.43</b>	<b>85.98±1.73</b>	<b>61.91±1.45</b>	<b>71.97±1.97</b>	<b>65.89±2.08</b>	53.87±1.85



**Figure 6:** The components clustering results based on different physical information, that are,  $\{x, y, A, L, \bar{\varphi}, \alpha\}$ ,  $\{x, y, A\}$ ,  $\{x, y\}$  of ASC parameters, and  $\{Amp, Loc\}$  of the amplitude image, from top to bottom.

parameters, such as the full description of attributed centers  $\{x, y, A, L, \bar{\varphi}, \alpha\}$ , the location and complex amplitude  $\{x, y, A\}$ , and only the location  $\{x, y\}$ . As a comparison, we also attempt to use the backscattering intensity of the amplitude image, where the amplitude with each pixel is used for clustering to obtain the components. Fig. 6 shows the different components clustering results based on various physical information of a SAR target.

The recognition performances of PIHA enabled DenseNet-121 based on different physical information are recorded in Table 6. Compared to the baseline model, the PIHA module enhances performance regardless of the physical information, even if only the amplitude information is applied without the ASC model. The full description of the scattering centers offers more sufficient physical information of SAR target, and thus the PIHA based on  $\{x, y, A, L, \bar{\varphi}, \alpha\}$  obtains better performance than the ones based on  $\{x, y, A\}$  and  $\{x, y\}$ .

It demonstrates that the proposed PIHA can be formulated using diverse physical information, as long as it ensures the provision of local semantics for the target components. As a result, the PIHA enabled neural network can take flexible input without being restricted just to complex-valued data.

#### 4.6. Attention Visualization

We calculate the averaged channel weights for all test images in every  $10^\circ$  azimuth angle interval, as shown in Fig. 8. The x-axis represents channels and the y-axis denotes azimuth angles. The colorbar demonstrates the higher/lower attention weights in red/blue. The channel weights of data-driven SE and PASE based on different physical information are given.

As we can referred in the Fig. 8, the data-driven SE attention is less discriminating cross channels. The channel attention conveys what to pay attention to, that is, the importance of each channel's feature is modeled. In the deep layers, where the spatial information is discarded to a certain extent, the channel information contains rich semantics. Observing from each row, for example, the SE attention weights are with homogeneous high values for those targets with azimuth angles near  $220^\circ$ . It indicates that the data-driven SE is inclined to assign similar channel weights for each input SAR target image. As a comparison, the PASE attentions are more discriminative cross channels where each sub-group of channels represent a local semantic related to target component, especially for those targets near some specific azimuth angles such as  $90^\circ$ ,  $180^\circ$ , and  $270^\circ$ . Correspondingly, the recognition accuracies of PIHA-Net near these specific angles are prominently superior with SE-Net, as shown in Fig. 7. Additionally, PASE attention based on ASC parameters behaves remarkable distinctions along azimuth angles. It is well-known that SAR targets vary dramatically with azimuth angles, and the ASC model describes the target considering the changes of scattering center

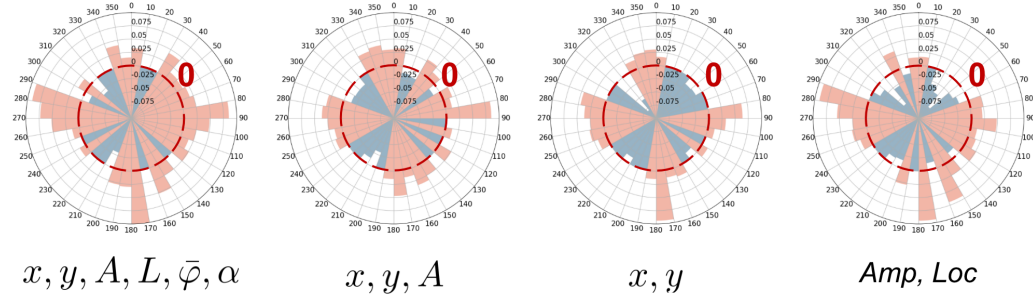


**Figure 7:** The recognition rate difference between the proposed hybrid attention PIHA and the data-driven SE attention model, displayed in the Coxcomb Chart to represent the results in every  $10^\circ$  azimuth angle. The red(blue) sectors indicate how much PIHA(SE) outperforms SE(PIHA).

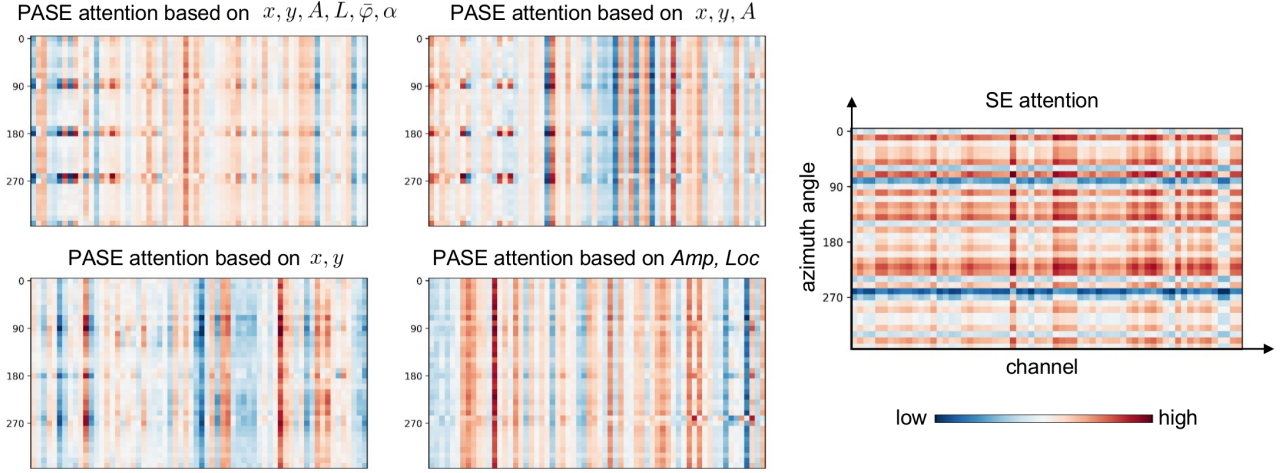


**Figure 8:** The attention visualization of different PASEs compared with the data-driven SE. We calculate the averaged channel weights for all targets in every  $10^\circ$  azimuth angle interval. The x-axis represents channels and the y-axis represents azimuth angle of target.

with azimuth looks. Consequently, the proposed physics-driven PASE is able to be aware of the physical parameters, and describes the semantic related channel weight more significantly. Notably, the PASE attention based on the full description of ASC model behaves much more discriminative than the ones based on less physical parameters. The  $(Amp, Loc)$  based PASE attention is rarely discriminating cross azimuth angles due to the simple physical information, but it still remains differentiation cross channels better than SE attention.

## 5. Conclusion

An effective approach to incorporating domain expertise involves designing a model architecture that complies with established scientific principles. For SAR targets, the combination of local components provides physically explainable semantics that should benefit target recognition. To this end, we propose a physics inspired hybrid attention mechanism where the design consideration is informed with a comprehensive understanding of SAR target characteristics. In order to evaluate the generalization ability of the method more rigorously, we propose the once-for-all evaluation protocol

where the model is trained once and tested on different test settings. The experiments investigate the effects of PIHA inserted into different deep architectures, and leveraging various types of physical information of SAR targets. In addition, the method is assessed with limited training samples and compared with the state-of-the-art approaches. We analyze the different working mechanisms between physics driven and data driven attentions in-depth. To contribute to the community, the physical information applied in this paper and the source code are available to public that ensures the reproducibility of our work and the fairness of comparing with other hybrid modeling approaches.

## 6. Acknowledgment

This work was supported by the National Natural Science Foundation of China under Grant 62101459, U20B2068, 62293543, and the China Postdoctoral Science Foundation under Grant BX2021248.

## References

- [1] A. Karpatne, G. Atluri, J. Faghmous, M. Steinbach, A. Banerjee, A. Ganguly, S. Shekhar, N. Samatova, and V. Kumar, "Theory-guided Data Science: A New Paradigm for Scientific Discovery from Data," *IEEE Transactions on Knowledge and Data Engineering*, vol. 29, no. 10, pp. 2318–2331, 2017.
- [2] L. von Rueden, S. Mayer, K. Beckh, B. Georgiev, S. Giesselbach, R. Heese, B. Kirsch, J. Pfrommer, A. Pick, R. Ramamurthy, M. Walczak, J. Garcke, C. Bauckhage, and J. Schuecker, "Informed Machine Learning – A Taxonomy and Survey of Integrating Prior Knowledge into Learning Systems," *IEEE Transactions on Knowledge and Data Engineering*, vol. 35, no. 1, pp. 614–633, Jan. 2023.
- [3] Z.-H. Zhou, "Open-environment machine learning," *National Science Review*, vol. 9, no. 8, p. nwa123, 2022.
- [4] S. Chen, H. Wang, F. Xu, and Y.-Q. Jin, "Target classification using the deep convolutional networks for sar images," *IEEE Transactions on Geoscience and Remote Sensing*, vol. 54, no. 8, pp. 4806–4817, 2016.
- [5] Sandia National Laboratory. (Accessed May 2023) 'The Air Force Moving and Stationary Target Recognition Database'. [Online]. Available: <https://www.sdms.af.mil/index.php?collection=mstar>
- [6] J. Liu, M. Xing, H. Yu, and G. Sun, "EFTL: Complex Convolutional Networks With Electromagnetic Feature Transfer Learning for SAR Target Recognition," *IEEE Transactions on Geoscience and Remote Sensing*, pp. 1–11, 2021.
- [7] J. Zhang, M. Xing, and Y. Xie, "FEC: A Feature Fusion Framework for SAR Target Recognition Based on Electromagnetic Scattering Features and Deep CNN Features," *IEEE Transactions on Geoscience and Remote Sensing*, vol. 59, no. 3, pp. 2174–2187, Mar. 2021.
- [8] S. Feng, K. Ji, L. Zhang, X. Ma, and G. Kuang, "SAR Target Classification Based on Integration of ASC Parts Model and Deep Learning Algorithm," *IEEE Journal of Selected Topics in Applied Earth Observations and Remote Sensing*, pp. 1–1, 2021.
- [9] Y. Li, L. Du, and D. Wei, "Multiscale CNN Based on Component Analysis for SAR ATR," *IEEE Transactions on Geoscience and Remote Sensing*, pp. 1–12, 2021.
- [10] Q. Liu and L. Lang, "MMFF: Multi-manifold feature fusion based neural networks for target recognition in complex-valued SAR imagery," *ISPRS Journal of Photogrammetry and Remote Sensing*, vol. 180, pp. 151–162, Oct. 2021.
- [11] J. Zhang, M. Xing, G.-C. Sun, and Z. Bao, "Integrating the reconstructed scattering center feature maps with deep cnn feature maps for automatic sar target recognition," *IEEE Geoscience and Remote Sensing Letters*, vol. 19, pp. 1–5, 2022.
- [12] Y. Li, L. Du, and D. Wei, "Multiscale cnn based on component analysis for sar atr," *IEEE Transactions on Geoscience and Remote Sensing*, vol. 60, pp. 1–12, 2022.
- [13] S. Feng, K. Ji, F. Wang, L. Zhang, X. Ma, and G. Kuang, "Pan: Part attention network integrating electromagnetic characteristics for interpretable sar vehicle target recognition," *IEEE Transactions on Geoscience and Remote Sensing*, vol. 61, pp. 1–17, 2023.
- [14] S. Feng, K. Ji, L. Zhang, X. Ma, and G. Kuang, "Sar target classification based on integration of asc parts model and deep learning algorithm," *IEEE Journal of Selected Topics in Applied Earth Observations and Remote Sensing*, vol. 14, pp. 10213–10225, 2021.
- [15] J.-H. Choi, M.-J. Lee, N.-H. Jeong, G. Lee, and K.-T. Kim, "Fusion of target and shadow regions for improved sar atr," *IEEE Transactions on Geoscience and Remote Sensing*, vol. 60, pp. 1–17, 2022.
- [16] S. Feng, K. Ji, L. Zhang, X. Ma, and G. Kuang, "Asc-parts model guided multi-level fusion network for sar target classification," in *IGARSS 2022 - 2022 IEEE International Geoscience and Remote Sensing Symposium*, 2022, pp. 5240–5243.
- [17] S. Feng, K. Ji, F. Wang, L. Zhang, X. Ma, and G. Kuang, "Electromagnetic scattering feature (esf) module embedded network based on asc model for robust and interpretable sar atr," *IEEE Transactions on Geoscience and Remote Sensing*, vol. 60, pp. 1–15, 2022.
- [18] J. Lv and Y. Liu, "Data augmentation based on attributed scattering centers to train robust cnn for sar atr," *IEEE Access*, vol. 7, pp. 25459–25473, 2019.
- [19] Z. Liu, L. Wang, Z. Wen, K. Li, and Q. Pan, "Multilevel scattering center and deep feature fusion learning framework for sar target recognition," *IEEE Transactions on Geoscience and Remote Sensing*, vol. 60, pp. 1–14, 2022.
- [20] C. Zhao, S. Zhang, R. Luo, S. Feng, and G. Kuang, "Scattering features spatial-structural association network for aircraft recognition in sar images," *IEEE Geoscience and Remote Sensing Letters*, vol. 20, pp. 1–5, 2023.
- [21] Z. Zeng, J. Sun, Z. Han, and W. Hong, "Sar automatic target recognition method based on multi-stream complex-valued networks," *IEEE Transactions on Geoscience and Remote Sensing*, vol. 60, pp. 1–18, 2022.
- [22] Y. Li and L. Du, "Design of the physically interpretable sar target recognition network combined with electromagnetic scattering characteristics," in *IGARSS 2022 - 2022 IEEE International Geoscience and Remote Sensing Symposium*, 2022, pp. 4988–4991.
- [23] J. Hu, L. Shen, and G. Sun, "Squeeze-and-excitation networks," in *2018 IEEE/CVF Conference on Computer Vision and Pattern Recognition*, 2018, pp. 7132–7141.
- [24] Q. Wang, B. Wu, P. Zhu, P. Li, W. Zuo, and Q. Hu, "Eca-net: Efficient channel attention for deep convolutional neural networks," in *2020 IEEE/CVF Conference on Computer Vision and Pattern Recognition (CVPR)*, 2020, pp. 11531–11539.
- [25] X. Li, W. Wang, X. Hu, and J. Yang, "Selective kernel networks," in *2019 IEEE/CVF Conference on Computer Vision and Pattern Recognition (CVPR)*, 2019, pp. 510–519.
- [26] H. Zhang, K. Zu, J. Lu, Y. Zou, and D. Meng, "Epsanet: An efficient pyramid squeeze attention block on convolutional neural network," in *Proceedings of the Asian Conference on Computer Vision (ACCV)*, December 2022, pp. 1161–1177.
- [27] Y. Chen, Y. Kalantidis, J. Li, S. Yan, and J. Feng, "A<sup>2</sup>-nets: Double attention networks," *Advances in neural information processing systems*, vol. 31, 2018.
- [28] S. Woo, J. Park, J.-Y. Lee, and I. S. Kweon, "Cbam: Convolutional block attention module," in *Proceedings of the European conference on computer vision (ECCV)*, 2018, pp. 3–19.
- [29] J. Park, S. Woo, J.-Y. Lee, and I.-S. Kweon, "Bam: Bottleneck attention module," *ArXiv*, vol. abs/1807.06514, 2018. [Online]. Available: <https://api.semanticscholar.org/CorpusID:49864419>
- [30] J. Fu, J. Liu, H. Tian, Y. Li, Y. Bao, Z. Fang, and H. Lu, "Dual attention network for scene segmentation," in *2019 IEEE/CVF Conference on Computer Vision and Pattern Recognition (CVPR)*, 2019, pp. 3141–3149.
- [31] Q.-L. Zhang and Y.-B. Yang, "Sa-net: Shuffle attention for deep convolutional neural networks," in *ICASSP 2021-2021 IEEE International Conference on Acoustics, Speech and Signal Processing (ICASSP)*. IEEE, 2021, pp. 2235–2239.
- [32] Y. Hao, Y. Zhang, K. Liu, S. He, Z. Liu, H. Wu, and J. Zhao, "An end-to-end model for question answering over knowledge base with cross-attention combining global knowledge," in *Proceedings of the 55th Annual Meeting of the Association for Computational Linguistics (Volume 1: Long Papers)*, 2017, pp. 221–231.
- [33] S. He, D. Sun, and Z. Wang, "Named entity recognition for chinese marine text with knowledge-based self-attention," *Multimedia Tools and Applications*, pp. 1–15, 2022.
- [34] Y. Fu, P. Xue, Z. Zhang, and E. Dong, "Pka 2-net: Prior knowledge-based active attention network for accurate pneumonia diagnosis on chest x-ray images," *IEEE Journal of Biomedical and Health Informatics*, 2023.
- [35] S. Hong, C. Xiao, T. Ma, H. Li, and J. Sun, "Mina: multilevel knowledge-guided attention for modeling electrocardiography signals," *arXiv preprint arXiv:1905.11333*, 2019.
- [36] Z. Huang, Z. Pan, and B. Lei, "What, where, and how to transfer in sar target recognition based on deep cnns," *IEEE Transactions on Geoscience and Remote Sensing*, vol. 58, no. 4, pp. 2324–2336, 2020.

- [37] Z. Huang, C. O. Dumitru, Z. Pan, B. Lei, and M. Datcu, "Classification of large-scale high-resolution sar images with deep transfer learning," *IEEE Geoscience and Remote Sensing Letters*, vol. 18, no. 1, pp. 107–111, 2021.
- [38] Z. Huang, M. Datcu, Z. Pan, X. Qiu, and B. Lei, "Hdec-tfa: An unsupervised learning approach for discovering physical scattering properties of single-polarized sar image," *IEEE Transactions on Geoscience and Remote Sensing*, vol. 59, no. 4, pp. 3054–3071, 2021.
- [39] M. Datcu, Z. Huang, A. Anghel, J. Zhao, and R. Cacoveanu, "Explainable, physics-aware, trustworthy artificial intelligence: A paradigm shift for synthetic aperture radar," *IEEE Geoscience and Remote Sensing Magazine*, vol. 11, no. 1, pp. 8–25, 2023.
- [40] Z. Huang, Y. Liu, X. Yao, J. Ren, and J. Han, "Uncertainty exploration: Toward explainable sar target detection," *IEEE Transactions on Geoscience and Remote Sensing*, vol. 61, pp. 1–14, 2023.
- [41] Z. Huang, X. Yao, and J. Han, "Progress and perspective on physically explainable deep learning for synthetic aperture radar image interpretation," *Journal of Radars*, vol. 11, no. 1, p. 107–125, 2022.
- [42] Z. Huang, X. Yao, Y. Liu, C. O. Dumitru, M. Datcu, and J. Han, "Physically explainable cnn for sar image classification," *ISPRS Journal of Photogrammetry and Remote Sensing*, vol. 190, pp. 25–37, 2022.
- [43] Z. Huang, M. Datcu, Z. Pan, and B. Lei, "Deep sar-net: Learning objects from signals," *ISPRS Journal of Photogrammetry and Remote Sensing*, vol. 161, pp. 179–193, 2020.
- [44] V. Nair and G. E. Hinton, "Rectified linear units improve restricted boltzmann machines," in *Proceedings of the 27th International Conference on International Conference on Machine Learning*, ser. ICML'10. Madison, WI, USA: Omnipress, 2010, p. 807–814.
- [45] C. Trabelsi, O. Bilaniuk, Y. Zhang, D. Serdyuk, S. Subramanian, J. F. Santos, S. Mehri, N. Rostamzadeh, Y. Bengio, and C. J. Pal, "Deep complex networks," 2018.
- [46] R. Chakraborty, J. Bouza, J. H. Manton, and B. C. Vemuri, "Manifold-net: A deep neural network for manifold-valued data with applications," *IEEE Transactions on Pattern Analysis and Machine Intelligence*, vol. 44, no. 2, pp. 799–810, 2022.
- [47] A. Bordes, N. Usunier, A. Garcia-Duran, J. Weston, and O. Yakhnenko, "Translating embeddings for modeling multi-relational data," *Advances in neural information processing systems*, vol. 26, 2013.
- [48] A. Kashani and S. S. Barold, "Significance of qrs complex duration in patients with heart failure," *Journal of the American College of Cardiology*, vol. 46, no. 12, pp. 2183–2192, 2005.
- [49] F. G. Yanowitz, "Introduction to ecg interpretation," *LDS Hospital and Intermountain Medical Center*, 2012.
- [50] L. von Rueden, S. Mayer, K. Beckh, B. Georgiev, S. Giesselbach, R. Heese, B. Kirsch, J. Pfrommer, A. Pick, R. Ramamurthy, M. Walczak, J. Garcke, C. Bauckhage, and J. Schuecker, "Informed machine learning – a taxonomy and survey of integrating prior knowledge into learning systems," *IEEE Transactions on Knowledge and Data Engineering*, vol. 35, no. 1, pp. 614–633, 2023.
- [51] H. Liu, B. Jiu, F. Li, and Y. Wang, "Attributed scattering center extraction algorithm based on sparse representation with dictionary refinement," *IEEE Transactions on Antennas and Propagation*, vol. 65, no. 5, pp. 2604–2614, 2017.
- [52] G. Huang, Z. Liu, L. Van Der Maaten, and K. Q. Weinberger, "Densely connected convolutional networks," in *2017 IEEE Conference on Computer Vision and Pattern Recognition (CVPR)*, 2017, pp. 2261–2269.
- [53] K. He, X. Zhang, S. Ren, and J. Sun, "Deep residual learning for image recognition," in *2016 IEEE Conference on Computer Vision and Pattern Recognition (CVPR)*, 2016, pp. 770–778.
- [54] M. J. Gerry, L. C. Potter, I. J. Gupta, and A. Van Der Merwe, "A parametric model for synthetic aperture radar measurements," *IEEE transactions on antennas and propagation*, vol. 47, no. 7, pp. 1179–1188, 1999.